Miniaturized gas ionization sensors using carbon nanotubes

Ashish Modi*, Nikhil Koratkar*, Eric Lass†, Bingqing Wei† & Pulickel M. Ajayan†

** Department of Mechanical, Aerospace and Nuclear Engineering, and*
† Department of Materials Science and Engineering, Rensselaer Polytechnic Institute, Troy, New York 12180, USA

Gas sensors operate by a variety of fundamentally different mechanisms[1–14]. Ionization sensors[13–14] work by fingerprinting the ionization characteristics of distinct gases, but they are limited by their huge, bulky architecture, high power consumption and risky high-voltage operation. Here we report the fabrication and successful testing of ionization microsensors featuring the electrical breakdown of a range of gases and gas mixtures at carbon nanotube tips. The sharp tips of nanotubes generate very high electric fields at relatively low voltages, lowering breakdown voltages several-fold in comparison to traditional electrodes, and thereby enabling compact, battery-powered and safe operation of such sensors. The sensors show good sensitivity and selectivity, and are unaffected by extraneous factors such as temperature, humidity, and gas flow. As such, the devices offer several practical advantages over previously reported nanotube sensor systems[15–17]. The simple, low-cost, sensors described here could be deployed for a variety of applications, such as environmental monitoring, sensing in chemical processing plants, and gas detection for counter-terrorism.

Various groups have explored the potential of carbon nanotubes for gas sensing, based on the electrical conductance changes of semiconducting nanotubes on exposure to gases[15–17]. Although this method has high sensitivity, it is limited by several factors, such as the inability to identify gases with low adsorption energies, poor diffusion kinetics or poor charge transfer with nanotubes. It is also challenging to use this technique to distinguish between gases or gas mixtures; gases in different concentrations could produce the same net change in conductance as produced by a single pure gas. Nanotube conductance is also very sensitive to changes in environmental conditions (moisture, temperature, gas-flow velocity), and chemisorption could cause irreversible changes in nanotube conductivity.

Figure 1 shows details of our sensor—a diagram of the component parts (Fig. 1a), and the configuration of the electrodes (Fig. 1b). Controlled d.c. voltage is applied between the anode (vertically aligned multiwalled nanotube—MWNT—film) and the cathode (Al sheet), which are separated by a glass insulator. The MWNT film (Fig. 1c) used for this test was grown by chemical vapour deposition[18–20] (CVD) on an SiO_2 substrate, as reported earlier. Nanotubes in the film are ~25–30 nm in diameter, ~30 μm long, with ~50 nm separation between nanotubes[20].

Individual MWNTs within the film, owing to their nanometre-scale tip radius ($R \approx 15$ nm), create very high nonlinear electric fields near the tips[21–24]. This hastens the breakdown process due to formation of a 'corona' or conducting filament of highly ionized gas that surrounds the MWNT tips. This corona promotes the formation of a powerful electron avalanche or plasma streamer that bridges the gap between the electrodes, and allows a self-sustaining interelectrode discharge to be created at relatively low voltages. The technique is very powerful for several reasons. (1) The precise breakdown voltage provides the 'fingerprint' for the gas to be identified; it is well established that at constant temperature and pressure every gas has a unique[25,26] breakdown electric field. (2) By monitoring the self-sustaining discharge current, the gas concentration can be determined. (3) Because this technique does not involve adsorption/desorption of gases, the sensor displays a fast response and is not limited by considerations of reversibility.

The device was first tested in air (Fig. 2a) with anode–cathode separation of 150 μm. Continuous current discharge of 460 μA was generated at 346 V. Tests were repeated with metal electrodes (no nanotubes), while still maintaining the electrode separation of 150 μm. For this case, breakdown voltage of air occurred at 960 V with current discharge of 69 μA. This shows that by the use of MWNTs as the anode, the breakdown of air can be reduced nearly 65%. The discharge current is also increased from 69 μA to 460 μA (~6-fold increase), leading to high sensitivity (discharge current at breakdown indicates concentration of the detected species, therefore a high discharge current enables detection of dilute concentrations of the unknown gas). We believe that the observed increase in discharge current is related to the high density of MWNTs that constitute the electrode surface (Fig. 1c). The billions of aligned nanotubes covering the substrate produce a consistent nanometre-scale surface topology unobtainable for conventional planar electrodes or micromachined electron emitters. A significant number of these tubes are expected to participate in ionization, leading to a more extensive conduction path and consequently higher discharge current. The devices were robust, with no degradation observed after hours of operation.

This nanotube-anode ionization device was used to detect the identity of several gas species, such as helium, argon, nitrogen, oxygen, carbon dioxide, ammonia and air. The nanotube device was placed in an environmental chamber with electrical feed-through, and air was pumped out of the chamber to establish a high vacuum (10^{-4} torr). The gas to be identified was then released in a controlled fashion. Breakdown data were recorded over a wide range of gas concentrations (10^{-7} to 10^{-1} mol l^{-1}). Figure 2b shows the breakdown voltages of several gases at room temperature (300 °K) and at a chamber pressure of 760 torr, that is, a gas concentration of 4×10^{-2} mol l^{-1}. For all tests shown, the anode–cathode separation was maintained at 150 μm. Note that each gas exhibits a distinct breakdown behaviour; helium displays the lowest (164 V) and ammonia shows the highest (430 V) breakdown voltage.

To study the effect of gas concentration, tests were conducted at

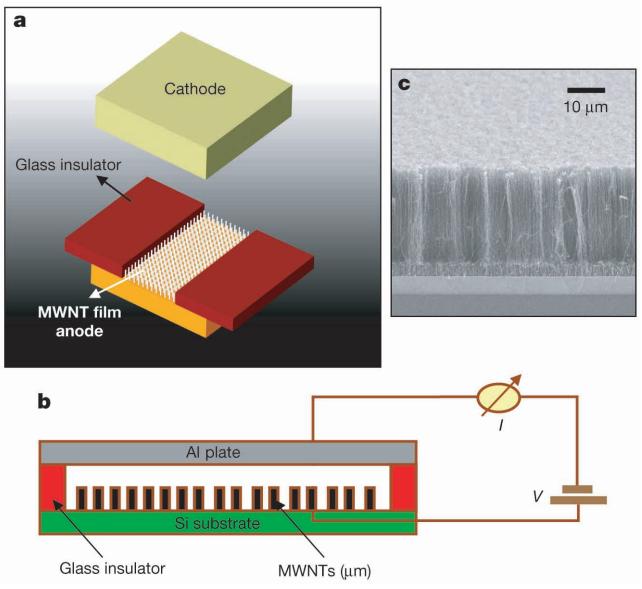

Figure 1 The nanotube sensor device. **a**, Exploded view of sensor showing MWNT film as the anode, 180-μm-thick glass insulator plates, and Al plate as cathode. **b**, Diagram of actual test set-up. **c**, SEM micrograph of a CVD-grown, vertically aligned MWNT film used as the anode.

reduced pressures (Fig. 3a, b). Figure 3a shows the effect of concentration on the breakdown voltages of air, argon, helium and ammonia. Note that the breakdown voltage does not vary significantly with gas pressure (the pressure is proportional to concentration for a fixed chamber volume). This is because breakdown behaviour in this case is dominated by the highly nonlinear electric field near the nanotube tips, resulting in a pre-breakdown plasma that helps to bridge the electrode gap and reduces the sensitivity of breakdown voltage to gas pressure. But at very low gas concentrations (below 10^{-6} mol l^{-1}), the breakdown voltage did increase as predicted by Paschen's law for uniform electric field[25,26], indicating a certain concentration threshold needed for the discharge to be self-sustaining. From Figs 2b and 3a we conclude that, for a fixed interelectrode spacing of the device, the breakdown voltage of each gas is unique and depends mainly on the electric field, being only weakly affected by concentration (this is valid over a wide range; Fig. 3a). Therefore by monitoring the breakdown voltage of the gas, its identity can be established. Note that species such as NH_3 and He that have large separation in breakdown voltage (Fig. 2b) are easier to distinguish than, say, NH_3 and O_2.

Figure 3b shows the self-sustaining current discharge at breakdown for argon, nitrogen, oxygen, ammonia and air. The discharge current varies logarithmically with concentration. This trend is valid over a wide range of gas concentrations, ranging from 10^{-7} to 10^{-1} mol l^{-1}. This shows that the self-sustaining discharge current generated at breakdown is a characteristic property of the number of gas molecules per unit volume that are available for conduction. For example, Fig. 3b indicates that for N_2 a current discharge of 328 μA corresponds to a concentration of 3.22×10^{-5} mol l^{-1}. The discharge current increases logarithmically to about 420 μA as the N_2 concentration is increased to 4×10^{-2} mol l^{-1}. Therefore the discharge current provides a convenient means to quantify the concentration of the species being detected. Figure 3b also shows that no hysteresis is observed in the sensor response, even for species such as NH_3 and O_2 that are known to interact strongly[15–17] with nanotube surfaces at room temperature.

The breakdown process described earlier propagates through the formation of a positive or negative corona, depending on whether the MWNT film is configured as the anode or the cathode. For the experiments with the MWNT film as anode, the breakdown propagation mechanism is via the formation of a positive corona. We also conducted experiments in air with the MWNT film as

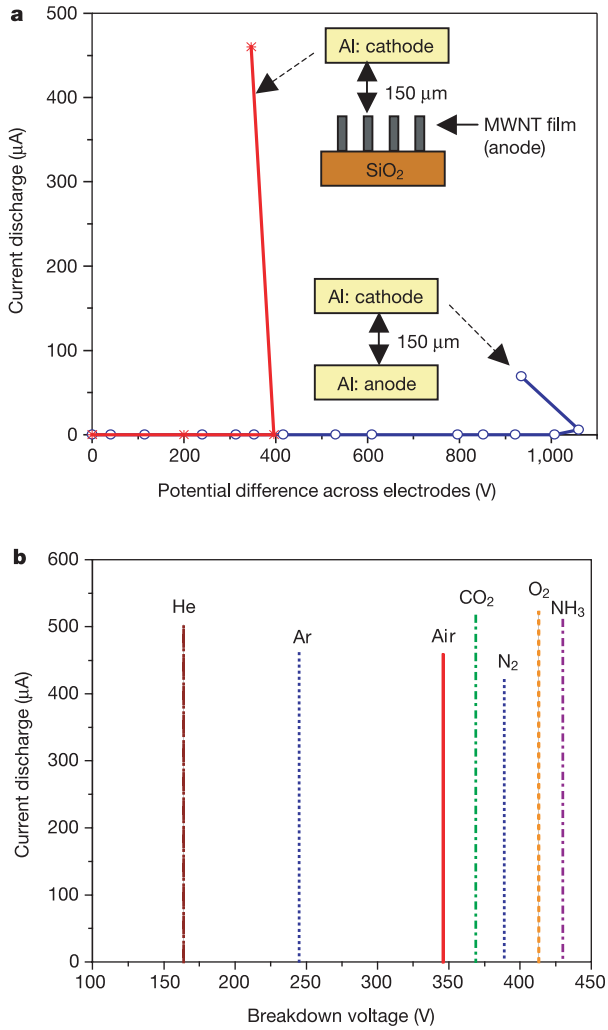

Figure 2 Current–voltage (*I–V*) curves for electrical breakdown. **a**, *I–V* curve (blue) with Al plate as the anode, separated from cathode by 150 μm, showing breakdown voltage of air at 960 V with discharge current of 69 μA; with MWNT film as anode (red) showing breakdown voltage of air at 346 V with discharge current of 460 μA. **b**, *I–V* curves for NH_3, CO_2, N_2, O_2, He, Ar and air, showing distinct breakdown voltages; ammonia displays the highest breakdown voltage, and helium the lowest.

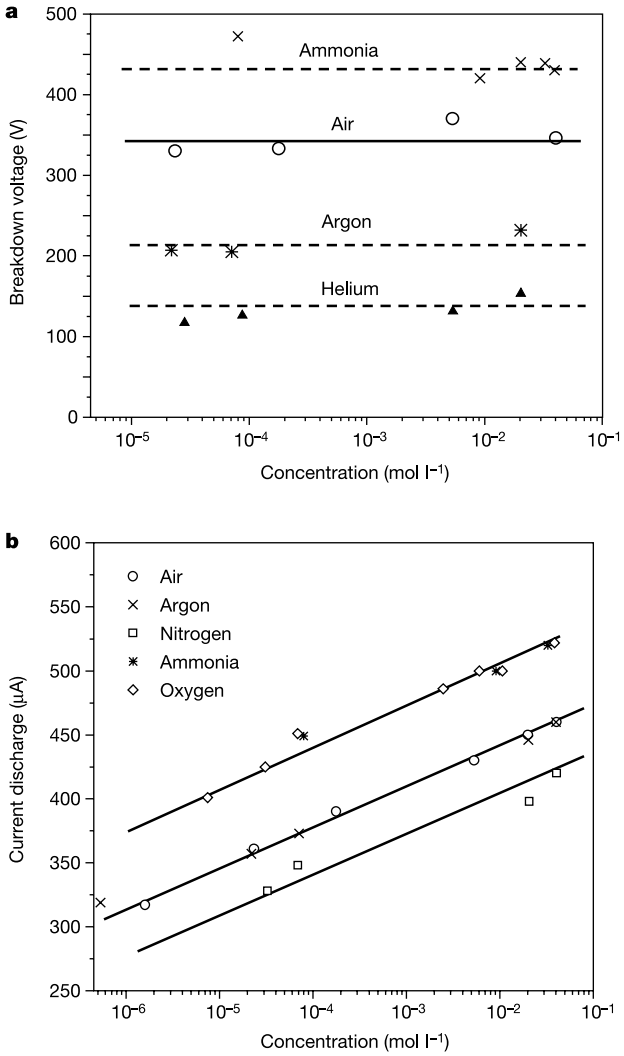

Figure 3 Effect of gas concentration on electrical breakdown. **a**, Breakdown voltage as a function of concentration; breakdown voltages vary only slightly with gas concentration. **b**, Discharge current at breakdown as a function of gas concentration. The discharge current varies logarithmically with concentration.

cathode (negative corona). The tests indicate that the voltage at which breakdown is initiated is similar for both positive (350 V) and negative (330 V) corona; but in negative corona, the breakdown voltage decreases to a lower value (~280 V) once breakdown is established. We believe that this is because once ionization is initiated in a negative corona, free electrons are repelled away from nanotube tips into the surrounding gas, triggering secondary ionizations that enable a self-propagating electron avalanche (a conducting path) to form at a lower electric field.

The breakdown voltage was found to become lower as the interelectrode spacing was reduced. This is expected, as reducing the electrode separation increases the electric field in the gap. Figure 4a shows breakdown voltage as a function of electrode separation. Two cases are shown, one when both electrodes were made out of Al plates and the other with the MWNT film as cathode. For the Al cathode, breakdown voltages came down from 1,050 V at 150 μm separation to 354 V at 28 μm separation; for the MWNT-film cathode, breakdown voltages went down from 280 V (at 150 μm separation) to 130 V (at 25 μm separation). Such voltages can be easily obtained by connecting six 22.5 V carbon–zinc batteries in series, suggesting that portable nanotube sensors based on the above idea could be made and utilized.

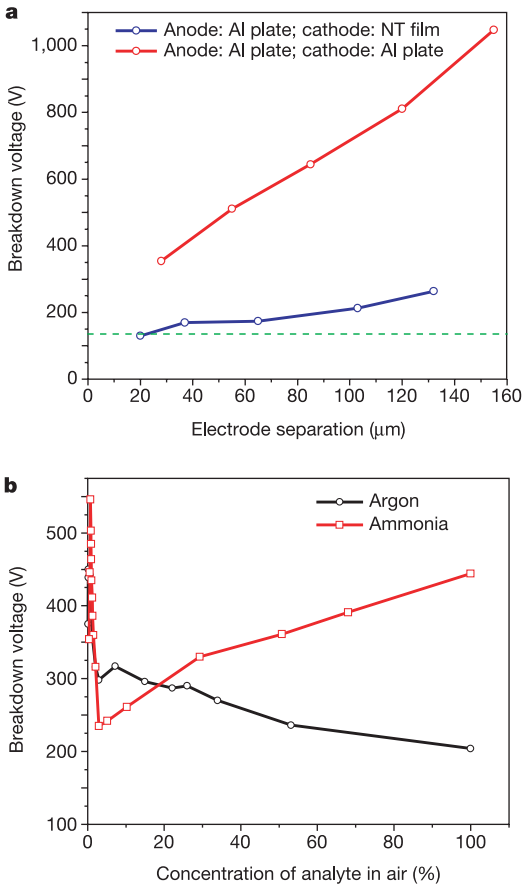

Figure 4 Effect of electrode separation, and detection of gases in mixtures. **a**, Breakdown voltage of air versus interelectrode separation. Breakdown voltages reduced from 280 V at 150 μm separation, to 130 V at 25 μm separation, for an MWNT cathode, and reduced from 1,050 V at 150 μm separation, to 354 V at 28 μm separation, for an Al cathode. Green line indicates the voltage obtained by connecting six, 22.5 V carbon–zinc batteries (Eveready AAA) in series. **b**, Breakdown of Ar and NH_3 in a mixture with air (MWNT film is configured as the anode, and interelectrode gap is 150 μm). Breakdown voltage increases with decreasing Ar concentration in the mixture. Breakdown of Ar ceases at about 1% concentration, and the breakdown voltage ramps up to that of pure air. For NH_3, the breakdown voltage decreases with decreasing NH_3 concentration until about 1%, beyond which the breakdown behaviour is identical to that of pure air.

Ionization sensors such as photo-ionization detectors (PID), flame-ionization detectors (FID) or electron-capture detectors (ECD) are not suitable for direct application to gas mixtures. These detectors work in conjunction with a gas-chromatography set-up that separates the mixture into distinct bands that can then be qualitatively and quantitatively analysed. The nanotube ionization sensor can be used to monitor gas mixtures without the direct use of a chromatography arrangement. Figure 4b shows the results for an Ar–air mixture with several different relative concentrations of the component gases. As expected, for over 50% Ar in the mixture, the breakdown voltage is nearly the same as that of pure Ar. As the relative concentration of Ar in the mixture is reduced, the breakdown voltage increases from about 250 V (for 50% Ar) to about 300 V (for 1% Ar). This is because air has a higher breakdown voltage than Ar, so the presence of air molecules tends to impede the breakdown of Ar. Below 1% concentration, the breakdown of Ar ceases and the breakdown voltage rises sharply to the value for pure air (~350 V). Similar results (detection limits ~1%) were also obtained for detection of NH_3 in a mixture with air (Fig. 4b). These tests indicate that the nanotube ionization microsensor (with proper calibration) shows promise for room-temperature detection of gases at the percentage level in mixtures with air with fast response (application of the breakdown electric field results in a stable discharge within ~20 μs; ref. 26). In contrast, the metal oxide sensors[2] used in industry typically operate at 300–500 °C for detection of 1% NH_3 with a response time of ~1 minute. Conducting polymer sensors[4] show detection limits of 1% for NH_3 at room temperature, but require ~10 minutes for sensing.

The nanotube ionization sensor can also be used as a detector in gas chromatographs, where sufficiently large analyte concentrations are at hand. In fact, the nanotube ionization detector could offer several advantages over the FID, PID or ECD detectors that are routinely used in chromatography sensors. FID has poor selectivity and requires bulky and hazardous hydrogen storage tanks during operation, PID with a better selectivity is limited to a small range of analytes, and ECD detectors are hazardous because they contain radioactive electron emitters. In contrast, the nanotube sensor is compact, safe to use and requires low power to operate. Since every gas has a characteristic breakdown electric field, a gas chromatograph with a nanotube ionization detector could potentially be applied to a broad range of analytes with good selectivity (Figs 2b, 3a).

To investigate the sensitivity range of a nanotube-chromatography sensor, we conducted a simulated gas-chromatography test with He chosen as the mobile phase. The results (Supplementary Information) indicate that, with appropriate design of the chromatography arrangement (including choice of mobile phase, stationary phase and process parameters), detection of analytes in the low p.p.m. range (~25 p.p.m.) appears feasible with this technique. Compact, low-power nanotube detectors coupled to miniature separation columns could potentially lead to truly field-portable gas chromatographs that could be used during emergency response and counter-terrorism situations that require definitive identification of contaminants in near real-time. □

Received 27 January; accepted 28 May 2003; doi:10.1038/nature01777.

1. Watson, J. & Ihokura, K. (eds) Special issue on gas sensing materials. *Mater. Res. Soc. Bull.* **24** (1999).
2. Shimizu, Y. & Egashira, M. Basic aspects and challenges of semiconductor gas sensors. *Mater. Res. Soc. Bull.* **24,** 18–24 (1999).
3. Takao, Y., Miyazaki, K., Shimizu, Y. & Egashira, M. High ammonia sensitive semiconductor gas sensors with double-layer structure and interface electrodes. *J. Electrochem. Soc.* **141,** 1028–1034 (1994).
4. Miasik, J., Hooper, A. & Tofield, B. Conducting polymer gas sensor. *J. Chem. Soc. Faraday Trans.* **182,** 1117–1126 (1986).
5. Capone, S., Mongelli, S., Rella, R., Siciliano, P. & Valli, L. Gas sensitivity measurements on NO_2 sensors based on copper (II) tetrakis (n-butylaminocarbonyl) phthalocyanine LB films. *Langmuir* **15,** 1748–1753 (1999).
6. Endres, H., Hartinger, R., Schwaiger, M., Gmelch, G. & Roth, M. A capacitive CO_2 sensor system with suppression of the humidity interference. *Sens. Actuators B* **57,** 83–87 (1999).

7. Lee, M. & Meyer, J. A new process for fabricating CO_2 sensing layers based on $BaTiO_3$ and additives. *Sens. Actuators B* **68,** 293–299 (2000).
8. Matsubara, S. *et al.* A practical capacitive type CO_2 sensor using CeO_2/$BaCO_3$/CuO ceramics. *Sens. Actuators B* **65,** 128–132 (2000).
9. Currie, J., Essalik, A. & Marusic, J. Micromachined thin film solid state electrochemical CO_2, NO_2 and SO_2 gas sensors. *Sens. Actuators B* **59,** 235–241 (1999).
10. Longergan, M. *et al.* Array-based vapor sensing using chemically sensitive, carbon black-polymer resistors. *Chem. Mater.* **8,** 2298–2312 (1996).
11. Dresselhaus, M., Dresselhaus, G. & Avouris, P. Carbon nanotubes — synthesis, structure, properties and applications. *Top. Appl. Phys.* **80,** 391–425 (2001).
12. Baughman, R. H., Zakhidov, A. A. & de Heer, W. A. Carbon nanotubes—the route toward applications. *Science* **297,** 787–792 (2002).
13. The Environmental Response Team. *Standard Operating Procedure No. 2114* (Environmental Protection Agency, Washington DC) ⟨http://www.ertresponse.com/sops/2114.pdf⟩ (1994).
14. Flame ionization detector, product data sheet (SRI Instruments, Torrance, CA) ⟨http://www.srigc.com/FID.pdf⟩ (1998).
15. Collins, P., Bradley, K., Ishigami, M. & Zettl, A. Extreme oxygen sensitivity of electronic properties of carbon nanotubes. *Science* **287,** 1801–1804 (2000).
16. Kong, J. *et al.* Nanotube molecular wires as chemical sensors. *Science* **287,** 622–625 (2000).
17. Peng, S., *et al.* in *3rd Int. Workshop on Structural Health Monitoring* (ed. Chang, F. K.) 1142–1148 (CRC Press, 2001).
18. Zhang, Z., Wei, B. Q., Ramanath, G. & Ajayan, P. M. Substrate-site selective growth of aligned carbon nanotubes. *Appl. Phys. Lett.* **77,** 3764–3766 (2000).
19. Wei, B. Q. *et al.* Organized assembly of carbon nanotubes. *Nature* **416,** 495–496 (2002).
20. Drotar, J. *et al.* Reflection high-energy electron diffraction from carbon nanotubes. *Phys. Rev. B* **64,** 125417 (2001).
21. de Heer, W. A., Chatelain, A. & Ugarte, D. A carbon nanotube field-emission electron source. *Science* **270,** 1179–1180 (1995).
22. de Jonge, N., Lamy, Y., Schoots, K. & Oosterkamp, T. H. High brightness electron beam from a multi-walled carbon nanotube. *Nature* **420,** 393–395 (2002).
23. Forbes, R. G., Edgcombe, C. J. & Valdre, U. Some comments on models for field enhancement. *Ultramicroscopy* **95,** 57–65 (2003).
24. Edgcombe, C. J. & Valdrè, U. Microscopy and computational modeling to elucidate the enhancement factor for field electron emitters. *J. Microsc.* **203,** 188–194 (2001).
25. Meek, J. & Craggs, J. *Electrical Breakdown of Gases* (Wiley and Sons, New York, 1978).
26. Abdel-Salam, M., *et al. High Voltage Engineering—Theory and Practice* (Dekker, New York, 2000).

Supplementary Information accompanies the paper on **www.nature.com/nature**.

Acknowledgements This work was supported by NSF (NSEC, NER awards), US Army Research Office, Philip Morris USA, and RPI.

Competing interests statement The authors declare that they have no competing financial interests.

Correspondence and requests for materials should be addressed to N.K. (koratn@rpi.edu) and P.M.A (ajayan@rpi.edu).

Unidirectional rotation in a mechanically interlocked molecular rotor

David A. Leigh*, Jenny K. Y. Wong*, François Dehez† & Francesco Zerbetto†

** School of Chemistry, University of Edinburgh, The King's Buildings, West Mains Road, Edinburgh EH9 3JJ, UK*
† Dipartimento di Chimica 'G. Ciamician', Universita degli Studi di Bologna, via F. Selmi 2, 40126 Bologna, Italy

Molecular motor proteins are ubiquitous in nature[1] and have inspired attempts to create artificial machines[2] that mimic their ability to produce controlled motion on the molecular level. A recent example of an artificial molecular rotor is a molecule undergoing a unidirectional 120° intramolecular rotation around a single bond[3,4]; another is a molecule capable of repetitive unimolecular rotation driven by multiple and successive isomerization of its central double bond[5–8]. Here we show that sequential and unidirectional rotation can also be induced in mechanically interlocked assemblies comprised of one or two small rings moving around one larger ring. The small rings in these [2]- and [3]catenanes[9] move in discrete steps between different binding sites located on the larger ring, with the movement driven by light, heat or chemical stimuli that change the relative affinity of the small rings for the different binding sites[10–12]. We find that the small ring in the [2]catenane moves with high positional integrity but without control over its direction of motion, while the two rings in the [3]catenane mutually block each other's movement to ensure an overall stimuli-induced unidirectional motion around the larger ring.

A [2]catenane in which one ring moves sequentially between three different binding sites ('stations') on the other ring is shown schematically in Fig. 1. A series of chemical reactions alters the thermodynamics of binding of two of the binding sites (switching them 'on' or 'off' in response to external stimuli) causing the small ring to move around the larger ring in successive steps in response to the changing global energy minimum. A hydrogen-bonded [2]catenane, **1**, based on this design was prepared together with the corresponding macrocycle, **2**, and [3]catenane (two of the small rings linked onto the bigger ring), **3**, as outlined in Fig. 2 and the Supplementary Information. The stations where the small rings non-covalently bind to the large ring were predicted to have widely differing macrocycle binding affinities (Fig. 3A): **A**, a secondary (2°) amide fumaramide group, should bind strongly because the *E*-olefin holds the amide carbonyls in a close-to-ideal geometry for intercomponent hydrogen bonding[10]; **B**, a tertiary (3°) amide fumaramide group, should bind less well than **A** because the extra methyl groups are bulky and some of the 3° amide bond rotamers will be sterically mismatched with the benzylic amide macrocycle[11]; **C**, a succinic amide ester, can still engage in double bifurcated hydrogen bonding, but will do so only weakly compared to **A** or **B** because it is flexible and one of the groups is an ester, which is a poor hydrogen bond acceptor[10,12]. A fourth station, an isolated amide group (shown as **D** in *E*,*E*-**3**) that can make fewer intercomponent hydrogen bonding contacts than **A**, **B** or **C**, is also present but only affects the behaviour of the [3]catenane. A benzophenone unit was attached to the highest-affinity fumaramide group to enable selective sensitized isomerization of that station at 350 nm (ref. 11).

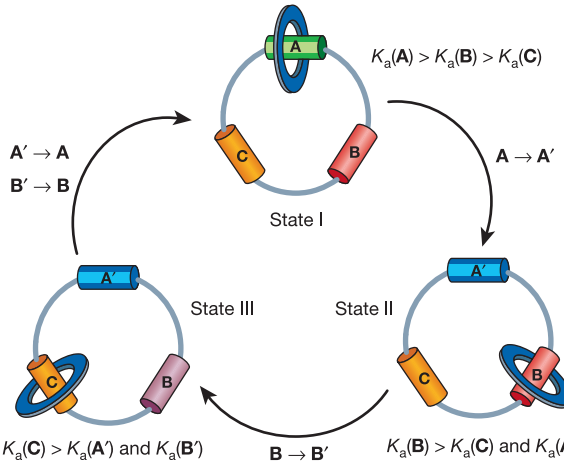

Figure 1 Stimuli-induced sequential movement of a macrocycle between three different binding sites in a [2]catenane. The larger macrocycle contains three stations, **A**, **B** and **C**, each with different binding affinities (association constants, K_a) for the smaller macrocycle such that K_a(**A**) > K_a(**B**) > K_a(**C**). Thus, in State I, the small macrocycle preferentially resides on station **A**. If binding site **A** is converted to **A′**, a group with a lower binding affinity for the macrocycle than **B** or **C**, then the small macrocycle will move through biased brownian motion to site **B** (State II). Similarly, if **B** is then changed into a station **B′** such that K_a(**B′**) < K_a(**C**) then the macrocycle will move to site **C** (State III). Finally, changing **A′** back to **A** and **B′** to **B** returns the small ring to its original position.